INTERNATIONAL JOURNAL FOR NUMERICAL METHODS IN FLUIDS
Int. J. Numer. Meth. Fluids 2008; **56**:1409–1415
Published online in Wiley InterScience (www.interscience.wiley.com). DOI: 10.1002/fld.1676

Numerical modelling of shear-thinning non-Newtonian flows in compliant vessels

M. Lukáčová-Medviďová[1,*,†] and A. Zaušková[1,2]

[1]*Institute of Numerical Simulation, Hamburg University of Technology, Hamburg, Germany*
[2]*Faculty of Mathematics, Physics and Informatics, Comenius University, Bratislava, Slovakia*

SUMMARY

The aim of this paper is to present recent results on numerical modelling of non-Newtonian flow in two-dimensional compliant vessels with application in hemodynamics. We consider two models of the shear-thinning non-Newtonian fluids and compare them with the Newtonian model. For the structure problem, the generalized string equation for radial symmetric tubes is used and extended to a stenosed vessel. A global iterative approach is used to approximate the fluid–structure interaction. At the end we present numerical experiments for selected non-Newtonian models, comparisons with the Newtonian model and the hemodynamic wall parameters: the wall shear stress and the oscillatory stress index.

Received 26 April 2007; Revised 15 October 2007; Accepted 18 October 2007

KEY WORDS: non-Newtonian fluids; fluid–structure interaction; shear-thinning flow; hemodynamic wall parameters; stenosis

1. INTRODUCTION

There are many numerical methods used in the blood flow simulation, which are based on the Newtonian model using the Navier–Stokes equations, see, e.g. [1–3]. On the other hand, in some cases, such as blood flow in small vessels or precise description of local flow effects, blood cannot be treated as the Newtonian fluid anymore and more precise models should be used, cf. [4–6]. In fact, blood is a complex rheological mixture showing several non-Newtonian properties, for example, shear thinning or viscoelasticity, cf., e.g. [5, 7, 8]. We address the significance of non-Newtonian models for reliable hemodynamical modelling. In particular, we will show that the rheological

*Correspondence to: M. Lukáčová-Medviďová, Institute of Numerical Simulation, Hamburg University of Technology, Schwarzenbergstrasse 95, 21073, Hamburg, Germany.
†E-mail: lukacova@tu-harburg.de

Contract/grant sponsor: European Union; contract/grant number: DEASE: MEST-CT-2005-021122

properties of fluid have influence on the wall deformation as well as on the hemodynamical wall indices, such as the wall shear stress (WSS) and the oscillatory shear index (OSI).

Consider a fluid motion governed by the momentum and the continuity equation:

$$\rho\partial_t \mathbf{v}+\rho(\mathbf{v}\cdot\nabla)\mathbf{v}-\mathrm{div}[2\mu(|D(\nabla\mathbf{v})|)D(\nabla\mathbf{v})]+\nabla p=0,\quad \mathrm{div}\,\mathbf{v}=0 \tag{1}$$

in two dimensions with ρ denoting the constant density of fluid, $\mathbf{v}=(v_1, v_2)$ the velocity vector, p the pressure, $D(\nabla\mathbf{v})=\frac{1}{2}(\nabla\mathbf{v}+\nabla\mathbf{v}^{\mathrm{T}})$ the symmetric deformation tensor and μ the viscosity of the fluid. The computational domain is a 2D radially symmetric channel given by a reference radius function $R_0(x_1)$ and an unknown free boundary function $\eta(x_1, t)$ describing the channel deformation. Owing to the symmetry we can restrict our computational domain to the upper half of the channel, $\Omega(\eta)\equiv\{(x_1, x_2, t):\ -L<x_1<L, 0<x_2<R_0(x_1)+\eta(x_1, t), 0<t<T\}$. The fluid and the geometry of the computational domain are coupled through the following Dirichlet boundary condition:

$$\mathbf{v}(x_1, R_0+\eta, t)=\frac{\partial\eta}{\partial t}\frac{\mathbf{n}}{|\mathbf{n}|}\quad \text{on } \Gamma^w \tag{2}$$

where $\Gamma^w=\{(x_1, x_2);\ x_1\in(-L, L), x_2=R_0(x_1)+\eta(x_1, t)\}$ is the deforming part of the boundary, $\mathbf{n}$ is the outward normal vector, $\mathbf{n}:=(-\partial_{x_1}R_0-\partial_{x_1}\eta, 1)$. Moreover, the normal component of the fluid stress tensor provides the forcing term for the deformation equation of the free boundary η:

$$\frac{\partial^2\eta}{\partial t^2}-\frac{|\sigma_{x_1}|}{\rho_w}\frac{\left(\dfrac{\partial^2\eta}{\partial x_1^2}+\dfrac{\partial^2 R_0}{\partial x_1^2}\right)}{\left[1+\left(\dfrac{\partial R_0}{\partial x_1}\right)^2\right]^{3/2}}+\frac{E\eta}{\rho_w(R_0+\eta)R_0}-c\frac{\partial^3\eta}{\partial t\partial^2 x_1}=\frac{(-\mathbf{T}_f\mathbf{n}\cdot\mathbf{e}_2-P_w)}{\rho_w h}\frac{R_0+\eta}{R_0} \tag{3}$$

$\mathbf{T}_f=-p\mathbf{I}+2\mu(|D(\nabla\mathbf{v})|)D(\nabla\mathbf{v})$. This is an extension of the generalized string model [9] derived for tubes with constant reference radius, see [10] for further details.

2. NON-NEWTONIAN MODELS FOR FLUID CONTROL QUANTITIES

Various non-Newtonian models for the blood flow can be found in the literature. In this paper we consider two non-Newtonian viscosity models: the Carreau model and the viscosity function of Yeleswarapu model, cf. [8]. In the Carreau model of shear-thinning fluid, the viscosity function depends on the deformation tensor in the following way:

$$\mu=\mu(|D(\nabla\mathbf{v})|)=\mu_\infty+(\mu_0-\mu_\infty)(1+|\gamma D(\nabla\mathbf{v})|^2)^q \tag{4}$$

where $q\leqslant 0$ and $\mu_0, \mu_\infty, \gamma$ are some given positive constants. In the case of $q=0$ the model reduces to the linear Newtonian model, i.e. the Navier–Stokes equations. The Yeleswarapu viscosity function reads

$$\mu=\mu(|D(\nabla\mathbf{v})|)=\mu_\infty+(\mu_0-\mu_\infty)\frac{\log(1+\gamma|D(\nabla\mathbf{v})|)+1}{(1+\gamma|D(\nabla\mathbf{v})|)} \tag{5}$$

DOI: 10.1002/fld

Several physical quantities have been introduced to describe some specific mechanism that could be correlated to intimal wall thickening. Many observations show that one reason is the blood flow oscillations during the diastolic phase of every single heart beat. Usually the WSS index and the OSI are studied [2]:

$$\mathrm{WSS} := \tau_w = -\mathbf{T}_f \mathbf{n} \cdot \boldsymbol{\tau}, \quad \mathrm{OSI} := \frac{1}{2}\left(1 - \frac{\int_0^T \tau_w \,\mathrm{d}t}{\int_0^T |\tau_w| \,\mathrm{d}t}\right) \tag{6}$$

Here $\mathbf{n}$ and $\boldsymbol{\tau}$ are the unit normal and the unit tangential vectors on Γ^w, respectively, and $[0, T)$ is the time interval of a single heart beat ($T \approx 1\,\mathrm{s}$).

3. DECOUPLING AND DISCRETIZATION METHODS

The fluid–structure interaction given by the right-hand side of the structure equation (3) and by boundary condition (2) is decoupled using a global iteration with respect to the domain geometry [3]. It means that in the kth iteration, $(\mathbf{v}^k, p^k, \eta^k)$ is obtained as a solution of (1) for all $(x, t) \in \Omega(\eta^{(k-1)})$ and (3) for all x_1. Instead of condition (2) we set $v_2(x_1, R_0 + \eta^{k-1}, t) = \partial\eta^{k-1}/\partial t = v_{\mathrm{grid}_2}$, $v_1 = 0$ on Γ^w, where $\mathbf{v}_{\mathrm{grid}}$ is the velocity of the mesh movement related to smoothing the grid after moving its boundary (we allow movement only in the direction of x_2, a movement in the direction of x_1 is neglected). We further linearize the nonlinear term in (3) by means of $E\eta/\rho_w(R_0 + \eta^{k-1})R_0$. In order to decouple (1) and (3), we evaluate the forcing term at the right-hand side of (3) at the old time step t_{n-1}. Convergence of this global method was experimentally justified. Our extensive numerical experiences show that two domain deformation iterations differ about $10^{-4}\,\mathrm{cm}$ pointwise after a few, about five iterations (for $R_0 \approx 1\,\mathrm{cm}$).

To approximate (1)–(3), we used the UG software toolbox [11] and extended it by implementing the non-Newtonian stress tensors as well as the approximation of the wall deformation given in (3). The problem class library for the Navier–Stokes equations in a moving domain is based on the ALE formulation. The spatial discretization of the fluid equations (1) was realized by the finite volume method with the pseudo-compressibility stabilization, see also [12] for other unsteady computation using this stabilization approach. The nonlinear convective term is linearized by the Newton method [12]. We used fixed point iterations for the linearization of the non-Newtonian stress tensor $\mu(|D(\nabla\mathbf{v})|)D(\nabla\mathbf{v}) \approx \mu(|D(\nabla\mathbf{v}^{\mathrm{old}})|)D(\nabla\mathbf{v})$, where $(.)^{\mathrm{old}}$ denotes the previous iteration [10].

In order to approximate the structure equation (3), we applied the Newmark scheme [1] in time and the second-order finite differences for the spatial approximation.

Physical meaning of quantities appearing in (3) is as follows, see [1]. The Young modulus is $E = 0.75 \times 10^5\,\mathrm{dynes\,cm^{-2}}$, the wall thickness $h = 0.1\,\mathrm{cm}$, the density of the vessel wall tissue $\rho_w = 1.1\,\mathrm{g\,cm^{-3}}$, $|\sigma_{x_1}| = G\kappa$, where $\kappa = 1$ is Timoshenko's shear correction factor and G is the shear modulus, $G = E/2(1+\sigma)$, where $\sigma = \frac{1}{2}$ for incompressible materials. The coefficient $c = \gamma/(\rho_w h)$, where we used $\gamma = 2 \times 10^4$.

In order to demonstrate the convergence of our numerical scheme, we present the convergence study in Table I. The experimental order of convergence is computed as $\mathrm{EOC} := \log_2[\|\mathbf{v}_h - \mathbf{v}_{h/2}\|_{L^2}/\|\mathbf{v}_{h/2} - \mathbf{v}_{h/4}\|_{L^2}]$, where $\mathbf{v}_h$ is the solution on the mesh with a size h. The computational domain $\Omega = [-5, 5] \times [0, 1]$ is divided consecutively into 16×2 elements (mesh 1), …, 128×16 elements (mesh 4). It should be pointed out that velocities are approximated by piecewise linear functions and the backward Euler method is used for time discretization of the fluid momentum

DOI: 10.1002/fld

Table I. Convergence study: the Carreu model with $q=-0.2$, $Re=80$.

	Rigid channel		Compliant channel		Compliant channel	
Mesh	$\|\mathbf{v}_h-\mathbf{v}_{h/2}\|_{L^2}$	EOC	$\|\mathbf{v}_h-\mathbf{v}_{h/2}\|_{L^2}$	EOC	$\|\eta_h-\eta_{h/2}\|_{L^2}$	EOC
1,2	0.6665857		0.5016501		0.002260504	
2,3	0.2709687	1.299	0.2647924	0.922	0.000907420	1.317
3,4	0.1322589	1.035	0.1287347	1.036	0.000475348	0.933

equation, see [3, 11]. Table I demonstrates the first-order convergence of the velocity and of the wall deformation in the $L^2((0,T)\times\Omega)$ norm for both rigid and compliant channels.

4. NUMERICAL EXPERIMENTS

We consider blood flow in a two-dimensional symmetric tube with a smooth-stenosed region. The impermeable moving wall Γ^w is modelled as a smooth-stenosed constriction [7]:

$$R_0(x_1)=1-\frac{g}{2}\left(1+\cos\left(\frac{\pi x_1}{2}\right)\right) \quad \text{if } x_1\in|r|; \quad R_0(x_1)=1 \quad \text{if } x_1\in(-L,-r)\cup(r,L)$$

where $L=5\,\mathrm{cm}$, $r=2\,\mathrm{cm}$ and $g=0.3$. These values give a stenosis with 30% area reduction corresponding to a relatively mild occlusion, which leads to a local small increment in the Reynolds numbers.

Let $\Gamma^{\mathrm{in}}=\{(-L,x_2);x_2\in(0,1)\}$, $\Gamma^{\mathrm{out}}=\{(L,x_2);x_2\in(0,1)\}$, $\Gamma^s=\{(x_1,0);x_1\in(-L,L)\}$ denote the inflow, outflow and symmetry boundaries, respectively. In order to obtain a reliable inflow boundary condition, we have firstly simulated flow in a rigid tube with parabolic inflow profile in space and a sine pulse wave $\sin^2(\pi t/\omega)$ with a period $\omega=1\,\mathrm{s}$ in time. The converged profile is then used as an inflow boundary condition for our problem. The symmetry condition $\partial_{x_1}v_1=0$, $v_2=0$ is prescribed on Γ^s and the Neumann-type boundary condition $\mathbf{T}_f\bar{m}\cdot\bar{e}_1=P_{\mathrm{out}}=0$, $v_2=0$ is given on Γ^{out}.

Owing to nonconstant behaviour of the viscosity, we have several possibilities to define the corresponding Reynolds number. In order to take into account the effect of both limiting viscosities, we define the Reynolds number Re using the average value $\overline{\mu}:=(\mu_0+\mu_\infty)/2$, i.e. $Re=\rho Vl/\overline{\mu}$. Here $\rho=1.0\,\mathrm{g\,cm^{-3}}$ is the fluid density, V is the characteristic velocity and l is the characteristic length (diameter of the tube). In the following experiments we chose, analogous to Nadau and Sequeira [7], $\mu_\infty=\frac{1}{2}\mu_0$, $\mu_0=1.26P$, $\mu_\infty=0.63P$, $\gamma=1$ in the Carreau (4) and the Yeleswarapu viscosity function (5). The corresponding $Re=80$.

The following figures illustrate comparisons of several aspects of the Newtonian and non-Newtonian flows in the straight channel and in the channel with a stenosed occlusion. Figure 1 describes the wall deformation function η at $t=0.36$ and $0.96\,\mathrm{s}$ for the straight (left) and the stenosed tube (right). Effects due to the presence of stenosis can be clearly observed. We can note

DOI: 10.1002/fld

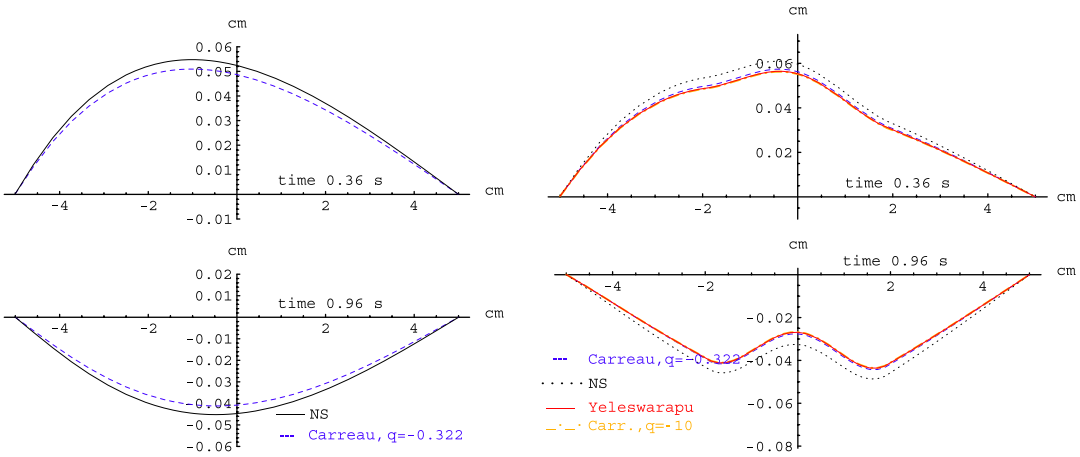

Figure 1. Wall deformation, left: the Newtonian (NS) and the Carreau models in the straight channel; right: the Newtonian (NS), the Yeleswarapu viscosity and the Carreau models in the stenosed channel.

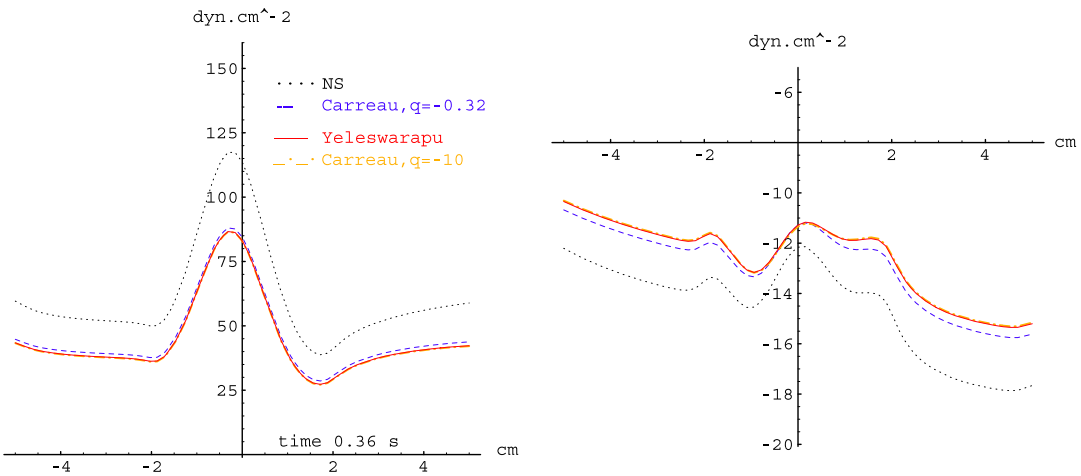

Figure 2. WSS: the Newtonian (NS), the Yeleswarapu viscosity function and the Carreau models.

that the two chosen non-Newtonian models yield comparable results for the domain deformation. A slightly different result can be seen if the Newtonian model is used.

Figure 2 describes the WSS distribution for the Newtonian and non-Newtonian fluids along the upper moving wall of a stenosed channel. Analogously as above we can see that the WSS depends considerably on the geometry. In fact, peaks in the WSS due to stenosis for both Newtonian and non-Newtonian models can be observed. Note that there are only marginal differences in the WSS between different non-Newtonian models. On the other hand, the differences between the Newtonian and the non-Newtonian models are more visible. As pointed out in [7], negative values of the WSS may indicate the existence of large recirculation zones and reversal flows around stenosis.

DOI: 10.1002/fld

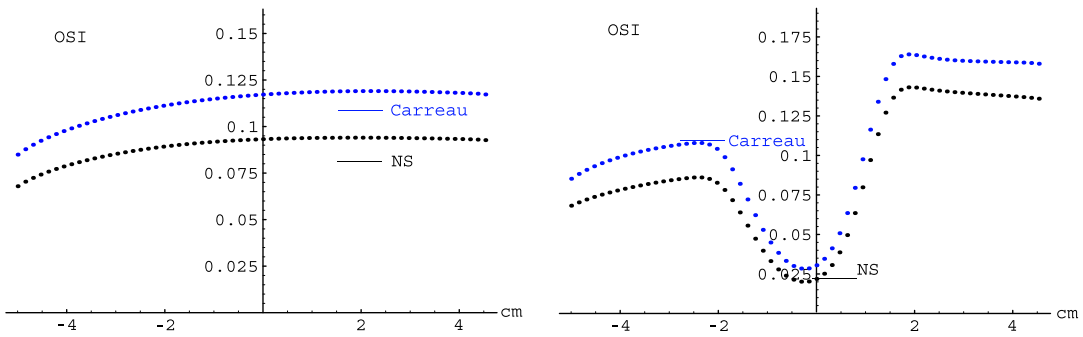

Figure 3. OSI indices computed using the Newtonian (NS) and the Carreau models with $q = -0.322$ in the straight channel (left) and in the stenosed channel (right).

Figure 3 compares the behaviour of the OSI for the straight and stenosed channels. We can observe different effects due to the presence of stenosis. High OSI values indicate the areas with increased danger of stenotic plug. The right picture in Figure 3 indicates that such areas appear at the end of stenotic reduction.

Our results confirm a considerable influence of the fluid rheology and the domain geometry on the wall deformation as well as on the hemodynamic wall parameters WSS and OSI.

ACKNOWLEDGEMENTS

This research has been financed by the 6th Framework Programme under contract no. DEASE: MEST-CT-2005-021122. The first author would like to thank Adélia Sequeira (IST, Lisbon) for fruitful discussions on the topic.

REFERENCES

1. Formaggia L, Gerbeau JF, Nobile F, Quarteroni A. On the coupling of 3D and 1D Navier–Stokes equations for flow problems in compliant vessels. *Computer Methods in Applied Mechanics and Engineering* 2001; **191**(6–7):561–582.
2. Quarteroni A, Gianluigi R. Optimal control and shape optimization of aorto-coronaric bypass anastomoses. *Mathematical Models and Methods in Applied Sciences* 2003; **13**(12):1801–1823.
3. Filo J, Zaušková A. 2D Navier–Stokes equations in a time dependent domain with Neumann type boundary conditions. *Journal of Mathematical Fluid Mechanics* 2007; accepted.
4. Abraham F, Behr M, Heikenschloss M. Shape optimization in steady blood flow: a numerical study of non-Newtonian effects. *Computer Methods in Biomechanics and Biomedical Engineering* 2005; **8**:127–137.
5. Anand M, Rajagopal KR. A shear-thinning viscoelastic blood model for describing the flow of blood. *International Journal of Cardiovascular Medicine and Science* 2004; **4**(2):59–68.
6. Gijsen FJH, van de Vosse FN, Jansen JD. Influence of the non-Newtonian properties of blood flow on the flow in large arteries: steady flow in a carotid bifurcation model. *Journal of Biomechanics* 1999; **32**:601–608.
7. Nadau L, Sequeira A. Numerical simulations of shear dependent viscoelastic flows with a combined finite element—finite volume method. *Computers and Mathematics with Applications* 2007; **53**(3–4):547–568.
8. Yeleswarapu KK, Kameneva MV, Rajagopal KR, Antaki JF. The flow of blood in tubes: theory and experiments. *Mechanical Research Communications* 1998; **25**(3):257–262.
9. Quarteroni A. *Fluid—Structure Interaction for Blood Flow Problems*. Lecture Notes on Simulation of Fluid and Structure Interaction, AMS-AMIF Summer School, Prague. European Mathematical Society: Charles University, Praque, 2001.

DOI: 10.1002/fld

10. Lukáčová-Medviďová M, Zaušková A. Mathematical and numerical modelling of complex fluid flow in compliant vessels. Preprint, 2007.
11. Bastian P, Johannsen K, Reichenberger V. *UG tutorial 1999*, revised 2002. http://hal.iwr.uni-heidelberg.de/~peter/Papers/tutorial.pdf.
12. Nägele S, Wittum G. On the influence of different stabilisation methods for incompressible Navier–Stokes equations. *Journal of Computational Physics* 2007; **224**:100–116.

DOI: 10.1002/fld